Journal Name

Dynamic Article Links ►

Cite this: DOI: 10.1039/c0xx00000x

www.rsc.org/xxxxxx

ARTICLE TYPE

Chemical Synthesis of Blue-emitting Metallic Zinc Nano-hexagons

Nguyen T. Mai, Trinh T. Thuy, Derrick M. Mott and Shinya Maenosono*

Received (in XXX, XXX) Xth XXXXXXXXX 20XX, Accepted Xth XXXXXXXXX 20XX
DOI: 10.1039/b000000x

We report a new ligand directed chemical synthesis of hexagonal shaped zinc nanoplates. The produced nano-hexagons (NHex)s display a thickness of about 20-40 nm and diameter ranging from about 200-350 nm, exhibiting a high aspect ratio. While zinc is traditionally highly susceptible to oxidation, these high surface area NHexs possess a remarkable resistance to atmospheric oxidation, owing to their unique surface crystalline faces and the fact that these particles are protected by organic surface ligands. The zinc NHexs size, morphology and chemical properties were characterized using transmission electron microscopy, scanning electron microscopy and X-ray photoelectron spectroscopy, among other techniques. Photoluminescence spectroscopy analysis revealed blue photoluminescence emission, making these NHexs potentially ideal for optics, optoelectronics or security printing.

Introduction

Low dimensional metal nanoparticles (NP)s are interesting due to the novel physical and chemical properties arising from the restricted nano-scale size, which can lead to many new and advanced applications.[1-4] The synthesis of metal NPs has received intensive study from physical techniques[1,2] to chemical approaches[5,6] to produce a wide range of NP based materials with a myriad of properties.[1-7] Low dimensional zinc NPs have been prepared primarily by physical methods such as metal thermal evaporation[8] or laser radiation technique,[9] but chemical methods such as electrochemical deposition[10] have also been employed. Zinc nanowires (one dimensional morphology) have also been formed by utilizing similar techniques.[11-13] Two dimensional zinc nanoplates were first synthesized using a micro-jet under electron-beam irradiation[14] and later by thermal evaporation[15] and vapor deposition techniques.[16] Recently, zinc submicron hexagonal plates fabricated on a Si(100) wafer by the hot-filament metal-oxide vapor deposition technique were found to exhibit both metal and semiconducting characteristics with light emission photoluminescence in the ultra-violet to visible range,[17] which is interesting for potential optical applications. It is noted that all the physical methods normally require high temperature (or high energy radiation) and until now the resulting zinc submicron plates have a diameter larger than 500 nm and a thickness larger than 100 nm.[14-17] In addition, zinc particles synthesized by physical methods always require a solid substrate as a place for the particle formation, and thus, cannot be redispersed in liquid to form particulate inks.

Chemical methods, on the other hand, have succeeded in the synthesis of noble metal NPs such as gold, silver, platinum, palladium and their alloys with capability in control of size and shape over a wide range.[5,18] However, for metals that have a high propensity for oxidation, such as aluminum (Al) or zinc (Zn), only few chemical synthesis techniques have been developed.[19,20] Up to now there is no report for the synthesis of anisotropic zinc nanoplates using a chemical approach that offers control over the size and shape of the resulting particles. From a fundamental standpoint, it would be highly interesting to study the properties of zinc NPs with size parameters less than 100 nm, because this is the size regime where the most pronounced size related properties occur. To achieve this, we developed a new ligand directed chemical synthesis approach to zinc nanoplates with a diameter less than 500 nm and thickness less than 50 nm. The resulting zinc NPs display remarkable photoluminescent properties induced by the nanoscale size. These small photoluminescent particles could be readily employed to create a fluorescent ink, which would not contain any rare earth and/or toxic elements. Such an ink would be ideal for use in security printing technology such as for secret barcoding or other optical applications. The origin of the unique optical properties is studied along with a brief discussion on the formation mechanism of the particles.

Experimental Section

Chemicals

$ZnCl_2$ (purity 98%), oleylamine (OAM, purity 70%), diphenylether (PhE, purity 99%), and lithium triethylborohydride (lithium super-hydride, $[LiEt_3]BH$, 1M solution in THF), as well as common solvents were purchased from Sigma Aldrich Corporation and used without further purification.

Synthesis of zinc nano-hexagons

1 millimole of $ZnCl_2$ and 30 millimoles of OAM were added to 20 mL of PhE in a 3 neck flask under Ar gas. The flask was then opened and heated up to 120 ºC for 20 min, after that, the flask was closed and heated to 200 ºC. When the temperature reached 200 ºC, lithium super-hydride was injected into the flask (2 millimoles), the solution quickly turned to black. The flask was

kept at 200 ºC for 20 min, then was quickly cooled down to room temperature. Ethanol was added to the NP reaction mixture which was then centrifuged at 4,500 rpm for 5 minutes to induce precipitation of the zinc NHexs. The cleaning process was repeated several times and the final dried and purified NHexs were collected for further investigation.

Characterization

Transmission Electron Microscopy (TEM) and High Resolution TEM (HRTEM) analysis was performed on Hitachi H-7650 and H-9000NAR transmission electron microscopes operated at 100 kV and 300 kV, respectively. Purified NHexs were suspended in hexane or toluene with additional OAM to produce NHex dispersions. 10 μL of the NHex dispersion was dropped onto a carbon-coated copper TEM micro-grid and were completely dried in ambient conditions. Field Emission Scanning Electron Microscopy (FESEM) measurements were conducted on a Hitachi S-4800 instrument. FESEM samples were prepared by suspending the purified zinc NHexs in hexane and then dropping the suspension onto a silicon substrate with subsequent drying in air. X-ray diffraction (XRD) crystallography patterns were collected on a Rigaku SmartLab X-ray diffractometer operated in reflection geometry at room temperature with Cu Kα radiation (1.5418 Å). X-ray Photoelectron Spectroscopy (XPS) was performed on a Shimadzu Kratos AXIS-ULTRA DLD high performance XPS system. Photoelectrons were excited by monochromated Al Kα radiation. Detection was done with a delay-line detector (DLD) and a concentric hemispherical analyzer (CHA). The pass energy of the CHA was 20 eV for narrow-scan spectra. The analyzed area on the specimen surface was 300×700 μm^2 and was located in the center of the irradiated region. The instrument was operated at a vacuum level of 1×10^{-8} Torr. XPS samples were prepared by depositing the dried and purified NPs onto conductive carbon tape. Photoluminescence (PL) spectra were collected on a Jasco FP-6300 spectrofluorimeter. Samples were prepared by re-dispersing the NPs into a mixture of toluene and hexane (1:1 volume ratio).

Results

The size and morphology of the resulting NPs was investigated using SEM and TEM techniques, as shown in Fig. 1. The NPs display a hexagonal shaped platelet morphology with a diameter of about 200-350 nm and of thickness of about 20-40 nm. Note that the average thicknesses estimated from TEM and SEM images are 40.0 ± 2.5 nm and 19.7 ± 1.1 nm, respectively. The SEM image (Fig. 1A) clearly shows the large scale area of nanoplates with hexagonal shape, demonstrating that the NPs have a uniform shape [hereafter referred to as nano-hexagons (NHex)s]. TEM images (Fig. 1B and C) were taken for several NHexs which often overlap with each other, illustrating the platelet morphology. The relative brightness of individual vs. overlapping NHexs (i.e. relatively light color for individual NPs) serves as a good indication that the particles are very thin. The rod-like NP found in Fig. 1C demonstrates a side view of a NHex arising from the parallel alignment of the NHex surface with the electron beam. We also found that by varying the feeding ratio between $ZnCl_2$ and OAM as well as reaction temperature, zinc NHexs with varying diameter and thickness can be prepared (for detail see ESI,† Figs. S1-3). The results demonstrate the versatility of the synthetic approach and reveal the remarkable enhanced optical properties for monometallic zinc NPs.

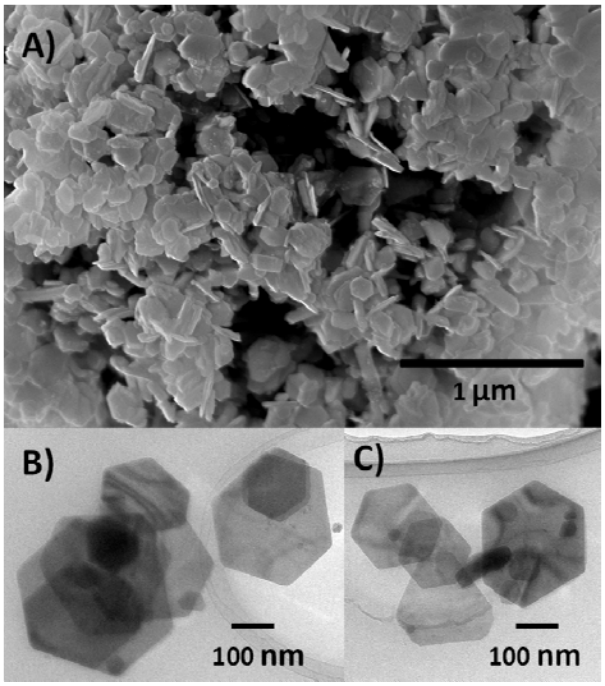

Fig. 1 SEM image (A) and TEM images (B and C) of zinc NHexs.

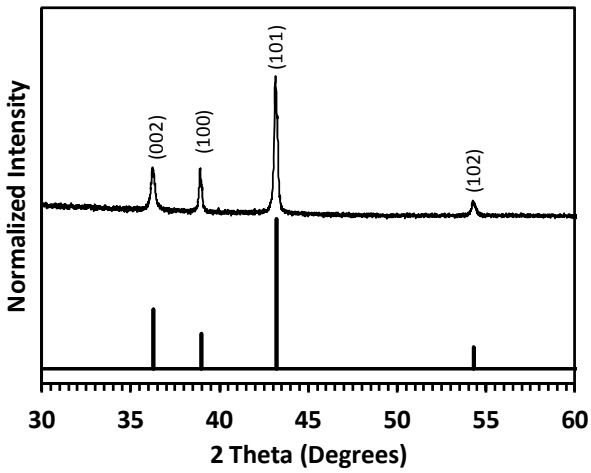

Fig. 2 XRD pattern of zinc NHexs with corresponding reference pattern for hexagonal phase zinc (JCPDS card number 03-065-5973).

The XRD pattern shown in Fig. 2 collected for the resulting NHexs shows peaks that are indexed with those of metallic zinc with hexagonal crystal structure. The diffraction peaks at 2θ = 36.2, 38.9, 43.1 and 54.2 degrees correspond to (002), (100), (101) and (102) lattice planes of hexagonal phase zinc, respectively.[21] It is important to note that no oxide phases were detected in the XRD pattern, which is somewhat unexpected because of the high propensity for zinc to oxidize, and because these NHexs have a relatively high surface area, which should enhance the oxidation. The XRD peaks observed in this analysis are broadened compared to that of the bulk counterpart, which is due to the relatively small crystalline size of the NHexs. The peak broadening of the (101) crystal plane was studied using the Scherrer equation (see ESI,† Eq. S1), and revealed a mean

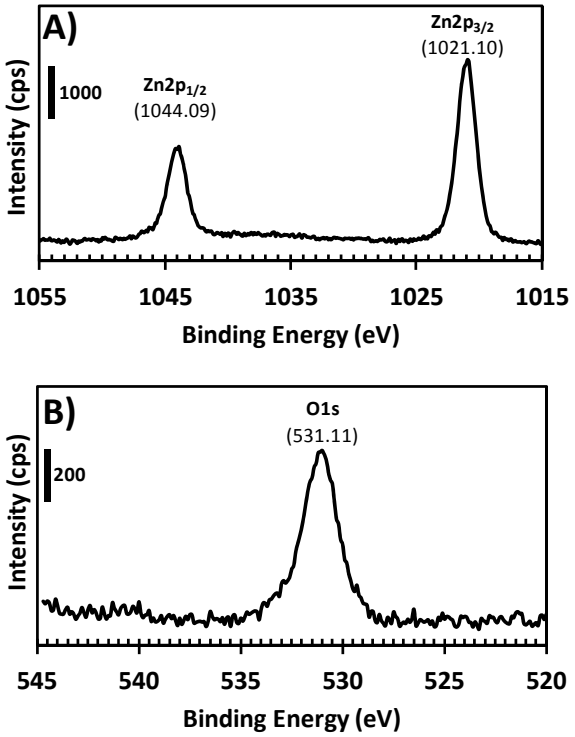

Fig. 3 XPS spectra of zinc NHexs in the Zn 2p (A) and O 1s (B) areas.

crystalline size of about 37 nm.[22] This result is in good agreement with the nominal size of the zinc NHexs (given that the particles are anisotropic in shape). Additionally, we found that the relative intensity of the (100) peak is slightly increased compared to that for bulk zinc metal, which may originate from the anisotropic shape of the zinc NHexs where the (100) crystalline planes may become more predominant in the nanocrystals over the counterpart bulk structure.

The XPS spectra shown in Fig. 3 were taken for the zinc 2p and oxygen 1s core level area of zinc NHexs to investigate their surface properties. The XPS peaks in the zinc 2p area are symmetrical with peak positions at 1021.10 and 1044.09 eV with a peak separation of 22.99 eV, which fits well with the reported values for Zn $2p_{3/2}$ and Zn $2p_{1/2}$ peaks for zinc metal. No sign of zinc oxide (Zn $2p_{3/2}$ and $2p_{1/2}$ peaks occurring at 1021.7 and 1044.8[23]) was found in the XPS spectrum. The oxygen 1s area shows a single low intensity peak at 531.11 eV arising from adventitiously adsorbed molecules in the sample, which supports the non-oxide nature of these zinc NHexs.

Fig. 4 shows the HRTEM images and electron diffraction pattern taken for a single zinc NHex. The lattice fringes along the face of the nanocrystal could be visualized and were measured to have a spacing of 2.35 Å, which corresponds to the (100) crystalline plane of hexagonal zinc.[21] The selected area electron diffraction (SAED) pattern collected for a single zinc NHex clearly shows a 6-fold diffraction symmetry, which reflects the fact that the zinc NHexs are single hexagonal crystal in nature. The calculated values from the SAED patterns of outer and inner spots are 2.10 and 2.49 Å. The outer spots correspond to the d-spacing reference value of (101) planes (2.092 Å).[21] The inner spots with 6-fold symmetry correspond to a d-spacing of 2.49 Å, but could not be assigned to any of the crystal planes of zinc that can generate 6-fold symmetry. It is possible that these spots originate from stacking faults in the zinc atomic layers in the NHexs[24] which is often observed for gold, silver or palladium nanoplates.[25,26]

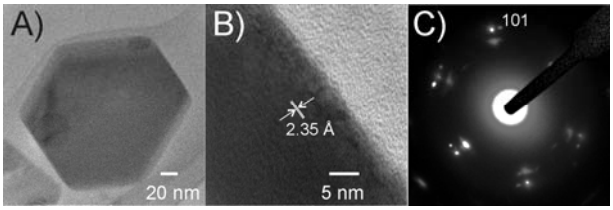

Fig. 4 HRTEM images (A and B) and selected area electron diffraction pattern (C) of a single zinc NHex.

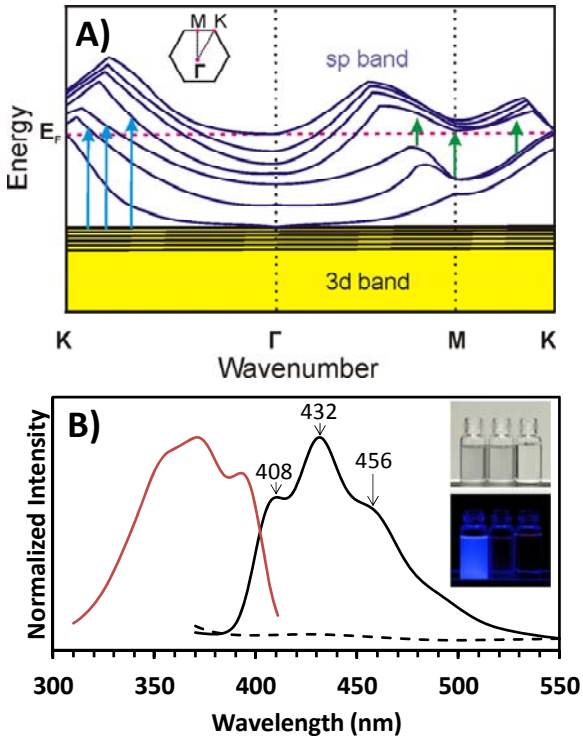

Fig. 5 (A) Schematic illustration for the band structure of zinc hexagonal plates drawn by reference from Fig. 4 in Ref. 17. Yellow region, violet curves, and pink dashed line correspond to 3d band, sp band, and the Fermi level, respectively. (B) Photoluminescence emission (black curve) and excitation (red curve) spectra of the zinc NHexs. The emission spectrum for oxidized zinc NHexs (dashed curve) is included. Excitation wavelength used for the emission spectra was 310 nm. Emission wavelength used for the excitation spectrum was 436 nm. The inset shows photographs of hexane/toluene 1:1 (vol/vol) dispersion of the zinc NHexs (left), hexane/toluene 1:1 (vol/vol) dispersion of the oxidized zinc NHexs (middle), and hexane/toluene 1:1 (vol/vol) (right) taken without (top) and with (bottom) UV illumination.

Discussion

Nanoparticle Shape Formation

We observe that in the presence of OAM, $ZnCl_2$ was dissolved in the phenylether to form a transparent solution which indicates the complex formation between $ZnCl_2$ and OAM. At high temperature, right after the injection of lithium superhydride, this complex was reduced to form metallic zinc (Zn*) which was indicated by the color of the reaction solution turning to black.

The reaction pathway to the reduction of zinc is given in equation 1. After this, zinc atoms undergo nucleation and growth in the solution to the final particle size and shape.

$$ZnCl_2 + 2Li[Et_3BH] \rightarrow Zn^* + 2LiCl + 2Et3B + H_2 \quad (1)$$

Because zinc NHexs have a hexagonal structure and it is known that the surface energy of {10$\bar{1}$0} prismatic planes of the hcp crystal is 1.5 times higher than the surface energy of {0001} basal planes which are normal to the c-axis,[27] the crystal growth rate will be faster for [01$\bar{1}$0], [10$\bar{1}$0] and [1$\bar{1}$00] directions to minimize the surface energy of the nanostructure.[15] In the case of the zinc NHexs synthesized here, the same phenomenon occurs with the zinc NHexs preferentially growing in the direction normal to prismatic planes (perpendicular to the c-axis), resulting in hexagonal shaped platelets. In the presence of capping molecules, the surfaces of the zinc NHexs are further stabilized, which further promotes the relatively thin platelet morphology.

Optical Properties

Recently, zinc submicron hexagonal plates were found to emit light of wavelength ranging from 312 to 700 nm in their photoluminescence spectrum.[17] The experimental and calculation results for the zinc hexagonal plates suggest that the size and shape lead to two special characteristics in their electronic structure: first, the energy offset between the Fermi level and upper level of the 3d band ($E_{F\text{-}3d}$) is smaller than that of bulk zinc metal, and second, the sp band itself is discretized to form the intraband gap ($E_{g(sp)} \sim 2.7$ eV) near the M-point as shown in Fig. 5A.[17] Due to the relatively smaller $E_{F\text{-}3d}$ of zinc submicron plates compared to that of the bulk counterpart, the electrons excited via the 3d–sp interband transition (indicated by blue arrows in Fig. 5A) will relax to their ground state emitting light in the UV to blue range, while bulk zinc metal does not emit visible light. The electrons excited via the sp–sp intraband transition (indicated by green arrows in Fig. 5A) will emit light in the green to red range when they relax, which is also not observed for bulk zinc metal.[17]

Fig. 5B shows the emission and excitation spectra of as-synthesized zinc NHexs. In the emission spectrum of the zinc NHexs, visible light emission can be observed from 390 nm to 550 nm with an excitation wavelength of 310 nm. The peaks located at 408, 432 and 456 nm correspond to 3.0, 2.9 and 2.7 eV. In addition, a shoulder is observed at around 490 nm which corresponds to 2.5 eV. In the reported data for thicker zinc submicron plates (diameter larger than 520 nm and thickness larger than 140 nm),[17] the emission peaks are located at 362, 400 and 458 nm corresponding to 3.4, 3.1 and 2.7 eV. Both emission peaks at 3.4 and 3.1 eV are assigned to the relaxation of electrons excited via the 3d–sp interband transition, while the emission at 2.7 eV is assigned to the relaxation of electrons excited via the sp–sp intraband transition.[17] To explain the origin of each peak in our case and the difference between our photoluminescence peak positions compared to the reported data for the zinc submicron plates, the following facts should be taken into account: (i) the zinc NHexs are much thinner (thickness of about 20-40 nm) compared to the zinc submicron plates (thickness larger than 100 nm), (ii) both calculation and experimental results show that $E_{F\text{-}3d}$ decreases when the size of zinc metal decreases from the bulk to nano size regime. Hence, there are three possibilities for the origin of the emission peaks in our photoluminescence spectrum. First, the peaks centered at 408 (3.0 eV) and 432 nm (2.9 eV) stem from the relaxation of electrons excited via the 3d–sp interband transition (blue arrows in Fig. 5A), while the peaks at 456 (2.7 eV) and 490 nm (2.5 eV) originate from the relaxation of electrons excited via the sp–sp interband transition (green arrows in Fig. 5A). Second, three emission peaks at 3.0, 2.9 and 2.7 eV arise from the 3d–sp interband transition due to the smaller $E_{F\text{-}3d}$ in our case in comparison to the zinc submicron plates, while the lowest-energy peak at 2.5 eV originates from the relaxation of electrons excited via the sp–sp interband transition. Third, all four emission peaks stem from the 3d–sp interband transition due to the much smaller $E_{F\text{-}3d}$ in our case in comparison to the zinc submicron plates. In any case, the zinc NHexs show fluorescence emission at a longer wavelength than zinc plates with a submicron size, and thus, they would have a higher degree of usability for practical applications than the zinc submicron plates.

Effect of Oxidation

To confirm the oxidation resistivity of the zinc NHexs and the effect of oxidation on their fluorescence property, the surfaces of the zinc NHexs were oxidized by exposing them to air for two weeks. The resulting zinc NHexs were analyzed by TEM, XPS and XRD (for detail see ESI,† Figs. S5-7), and it was clearly found that the surface of the zinc NHexs were partially oxidized after the treatment. Not surprisingly, the oxidized zinc NHexs do not show any fluorescence emission over the entire inspected range (dashed line, Fig. 5B), indicating that the surface oxidation of the zinc NHexs induces surface states acting as nonradiative recombination centers. The inset of Figure 5B shows photographs of a hexane/toluene 1:1 (vol/vol) dispersion of the zinc NHexs (left), hexane/toluene 1:1 (vol/vol) dispersion of the oxidized zinc NHexs (middle), and hexane/toluene 1:1 (vol/vol) (right) taken under room light (top) and UV illumination (bottom). It is readily apparent that the zinc NHexs emit blue light under the UV illumination, while the oxidized zinc NHexs do not. This photoluminescence property is intriguing, and with further processing the understanding of these optical properties may lead to new optical devices or applications.

Conclusions

In conclusion, we developed a chemical synthesis approach towards pure zinc nano-hexagons (NHex)s with a mean diameter of 200-350 nm and thickness of 20-40 nm. The synthesized zinc NHexs are remarkably resistant to oxidation, which is surprising given the fact that bulk zinc readily oxidizes in the atmosphere, and the materials produced here have a relatively large surface area. This oxidation resistance arises from the unique crystalline surface properties of the anisotropic NPs, and the organic molecule encapsulating species protecting the particle surfaces. The zinc NHexs possess both metallic and semiconducting characteristics, and thus, exhibit blue fluorescence emission, which has the potential to be used in applications such as optics and/or optoelectronics. Further investigation of synthetic conditions may offer enhanced control over the NPs size, shape oxidation property and other properties and characteristics. The ongoing work includes further studies on the fluorescence of Zn NHexs with different sizes, fluorescence quantum yield,

fluorescence life time, and improvement of size uniformity of zinc NHexs based on further understanding of how to control the morphology of the NPs.

Notes and references

School of Materials Science, Japan Advanced Institute of Science and Technology, 1-1 Asahidai, Nomi, Ishikawa 923-1292, Japan. E-mail: shinya@jaist.ac.jp

† Electronic Supplementary Information (ESI) available: Additional TEM images of zinc nano-hexagons, the Scherrer equation, UV-Vis spectrum, results for partial oxidation of zinc nano-hexagons when exposed to the air, and results for zinc nano-hexagons synthesized using feeding ratio of Zn:OAM = 1:2. See DOI: 10.1039/b000000x/

1 K. Watanabe, D. Menzel, N. Nilius and H. J. Freund, *Chem. Rev.*, 2006, **106**, 4301.

2 C. N. R. Rao, G. U. Kulkarni , P. J. Thomas and P. P. Edwards, *Chem. Soc. Rev.*, 2000, **29**, 27.

3 A. B. Evlyukhin, C. Reinhardt, U. Zywietz and B. N. Chichkov, *Phys. Rev. B*, 2012, **85**, 245411.

4 H. Kobayashi, M. Yamauchi, H. Kitagawa, Y. Kubota, K. Kato and M. Takata, *J. Am. Chem. Soc.*, 2010, **132**, 5576.

5 B. Wiley, Y. Sun and Y. Xia, *Acc. Chem. Res.*, 2007, **40**, 1067.

6 L. Wang and Y. Yamauchi, *J. Am. Chem. Soc.*, 2010, **132**, 13636.

7 *Complex-Shaped Metal Nanoparticles: Bottom-Up Syntheses and Applications*, ed. by T. K. Sau and A. L. Rogach, Wiley-VCH 2012.

8 K. Aslan, M. J. R. Previte, Y. Zhang and C. D. Geddes, *J. Phys. Chem. C*, 2008, **112**, 18368.

9 E. H. Khan, S. C. Langford, J. T. Dickinson, L. A. Boatner and W. P. Hess, *Langmuir*, 2009, **25**, 1930.

10 B. N. Pal and D. Chakravorty, *J. Phys. Chem. B*, 2006, **110**, 20917.

11 J.-G. Wang, M.-L. Tian, N. Kumar and T. E. Mallouk, *Nano Lett.*, 2005, **5**, 1247.

12 S. Kar, T. Ghoshal and S. Chaudhuri, *Chem. Phys. Lett.*, 2006, **419**, 174.

13 R. Cong, Q. Wang, J. Zhang, J. Wang, Y. Xu, Y. Jin and Q. Cui, *Mater. Chem. Phys.*, 2011, **129**, 611.

14 J. Gong, S. Yang, H. Huang, X. Zhao and Z.-Z. Yu, *Nanotechnology*, 2007, **18**, 235606.

15 D. Yuvaraj, K. N. Rao and K. Barai, *Solid State Commun.*, 2009, **149**, 349.

16 R. S. Devan, J.-H. Lin, Y.-J. Huang, C.-C. Yang, S. Y. Wu, Y. Liou and Y.-R. Ma, *Nanoscale*, 2011, **3**, 4339.

17 J.-H. Lin, Y.-J. Huang, Y.-P. Su, C.-A. Liu, R. S. Devan, C.-H. Ho, Y.-P. Wang, H.-W. Lee, C.-M. Chang, Y. Liou and Y.-R. Ma, *RSC Adv.*, 2012, **2**, 2123.

18 J. Yang , J. Yang and J. Y. Ying, *ACS Nano*, 2012, **6**, 9373.

19 S. Chandra and A. Kumar, *Spectrochim. Acta, Part A*, 2012, **97**, 935.

20 C. S. Birkel, E. Mugnaioli, T. Gorelik, U. Kolb, M. Panthöfer and W. Tremel, *J. Am. Chem. Soc.*, 2010, **132**, 9881.

21 JCPDS No. 03-065-5973

22 P. Scherrer, *Göttinger Nachrichten Gesell.*, 1918, **2**, 98.

23 O. Lupan, L. Chow, T. Pauporté, L. K. Ono, B. R. Cuenya and G. Chai, *Sens. Actuators B*, 2012, **173**, 772.

24 P. G. Partridge, *Int. Mater. Rev.*, 1967, **12**, 169.

25 V. Germain, J. Li, D. Ingert, Z. L. Wang, M. P. Pileni, *J. Phys. Chem. B*, 2003, **107**, 8717.

26 Y. Xiong, J. M. McLellan, J. Chen, Y. Yin, Z.-Y. Li, Y. Xia, *J. Am. Chem. Soc.*, 2005, **127**, 17118.

27 Z. A. Matysina, *Mater. Chem. Phys.*, 1990, **60**, 70.